Superconductor Science and Technology

Comparative study of CSD-grown *RE*BCO films with different rare earth elements: processing windows and T_c

To cite this article: M Erbe *et al* 2020 *Supercond. Sci. Technol.* **33** 094002

OPEN ACCESS
IOP Publishing
Superconductor Science and Technology
Supercond. Sci. Technol. **33** (2020) 094002 (11pp)
https://doi.org/10.1088/1361-6668/ab9aa0

Comparative study of CSD-grown *RE*BCO films with different rare earth elements: processing windows and T_c

M Erbe[1], P Cayado[1], W Freitag[1], K Ackermann[1], M Langer[1], A Meledin[2,3], J Hänisch[1] and B Holzapfel[1]

[1] Karlsruhe Institute of Technology (KIT), Institute for Technical Physics (ITEP), Eggenstein-Leopoldshafen, Germany
[2] RWTH Aachen University, Central Facility for Electron Microscopy (GFE), Aachen, Germany
[3] Forschungszentrum Jülich GmbH, Ernst Ruska-Centre for Microscopy and Spectroscopy with Electrons (ER-C), Jülich, Germany

Received 15 November 2019, revised 6 March 2020
Accepted for publication 8 June 2020
Published 15 July 2020

Abstract

RE$Ba_2Cu_3O_{7-x}$ (*RE*BCO, *RE* = rare earth) compounds with different single *RE* elements were grown via TFA-MOD (metal-organic deposition of trifluoroacetates) to clarify their T_c values when grown by the same preparation method and their processing windows; here: the crystallisation temperatures at a constant process gas composition (pO_2, pH_2O). We focussed on the lanthanides (*Ln*) Nd, Sm, Gd, Dy, Ho, Er and Yb as substituents for Y in the *RE*BCO phase and investigated their growth behaviour in terms of resulting physical (inductive T_c and J_c(77 K)) and structural properties (determined by XRD, SEM, TEM). All phases were grown as pristine films on $LaAlO_3$ and $SrTiO_3$ and compared to their respective nanocomposites with 12 mol% $BaHfO_3$ for in-field pinning enhancement.

With regard to T_c and J_c(77 K), the optima of both values shift towards higher growth temperatures for increasing and decreasing *RE* ion size with respect to yttrium. Highest T_c values achieved so far do not show a trend that can solely be related to the *RE* ionic size. On the contrary, $T_{c,90}$ values of the *Ln*BCO compounds from Sm to Er range between 94.0 and 95.3 K and are, therefore, significantly larger than the highest values of the average-size non-lanthanide, Y, with $T_{c,90} = 91.5$ K. $J_{c,sf}$ values at 77 K seem to plateau between 5 and 6 MA cm^{-2} from Sm to Er and are again clearly above the maximum values we ever achieved for Y with 4.2 MA cm^{-2}. *RE*BCO phase formations of the very small Yb and large Nd turned out to be more difficult and require further adjustment of growth parameters. All *RE*BCO phases investigated here show distinct dependences of T_c on the lattice parameter *c*.

Keywords: REBCO, TFA-MOD, BHO nanocomposites, pinning, CSD

(Some figures may appear in colour only in the online journal)

1. Introduction

In order to assess the suitability of a *RE*$Ba_2Cu_3O_{7-x}$ (*RE*BCO or *RE*123, *RE* = rare earth) compound other than the well-established YBCO for coated conductor (CC) production, three main aspects have to be considered: price, process handling and performance. Moreover, all three have to be optimised simultaneously in order to raise the performance-cost ratio and make the material attractive for the market. Thus, CC production has to be cheap, simple and reproducible, and the product has to perform to the best of its possibilities and best at all operating conditions aimed for (i.e. temperature and magnetic field environment). But is there any room for

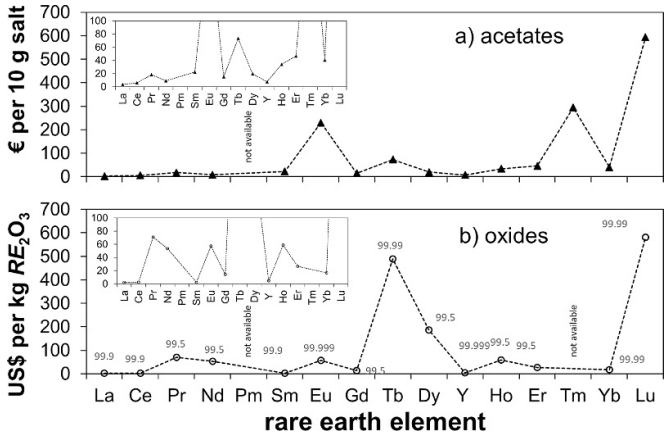

Figure 1. Prices of the rare earth compounds: (a) prices per 10 g *RE* acetate (99.9% purity grade) in Euro [12]; (b) world market prices per kg RE_2O_3 (for different available grades of purity as given in the graph above the data points) in US Dollar [13]; insets: magnifications to the low-cost region.

improvement beyond YBCO, when years of YBCO research have passed [1–11]?

YBCO is indeed one of the cheapest precursor media that can be purchased on the market. YBCO targets for pulsed laser deposition (PLD), for example, cost roughly half of a GdBCO target. The same applies for the prices of salts used for metal-organic deposition (MOD), figure 1(a). Here, yttrium is also one of the cheapest amongst all *RE* acetates. However, those prices probably reflect demand rather than possible production cost. If the demand of another *RE*BCO precursor was scaled to the demand of YBCO, prices might level, since world market prices for *RE* raw materials, figure 1(b), are only partially reflected in the prices of the precursor salts. Despite the rather cheap raw material for Eu, for example, the acetate is rather costly, while the overly expensive oxides of Tb and Dy have a rather low impact on the according costs of the acetates. Anyway, the pro rata cost for the rare earth element within the superconducting layer of a CC may rather be neglected when the entire production process is considered and prices for metallic substrates, buffer materials and processing costs are added to the sum.

Several thin film deposition methods have qualified for *RE*BCO CC production, such as physical vapour deposition techniques including PLD [14–16] and reactive co-evaporation [3, 16], as well as chemical methods including metal-organic chemical vapour deposition (MOCVD) [17] and chemical solution deposition (CSD) [6, 18]. All methods have their advantages and disadvantages, which have been examined carefully in several studies. Yet, when only the price is considered, techniques depending on high-vacuum equipment have clear disadvantages for large-scale production. Particularly cheap is the deposition from chemical solutions. CSD equipment consists of not more than a reel-to-reel-operated furnace with a deposition device, e.g. dip, spray, print or slot-dye coating. The entire CC architecture, including cap and buffer layers, can be processed 'all-chemically' [19]. However, with respect to the performance-cost ratio, mixed approaches may be the means of choice. Particularly, the deposition of the *RE*BCO layer via CSD has clear advantages over other techniques, though: The preparation of the precursor solutions is utterly simple and therefore cheap, and the composition can be easily altered through solution mixing or additions of further soluble salts. With this, a plethora of inclusions for pinning enhancement is accessible: atomic-scale doping [20] on the *RE* [21–23], the Ba [24–26], and the Cu [27–29] site or secondary phase additions of various compositions (e.g. Y_2O_3 [30], $BaZrO_3$ [31, 32], $BaHfO_3$ [33–35], $BaSnO_3$ [36], Ba_2YTaO_6 [37], Ba_2YNbO_6 [38]), forms (spherical, plate-like, rectangular, etc) and amount. Thereby, precipitates grown by CSD are known to lead to the largest reductions of the J_c anisotropy of *RE*BCO with sometimes near-isotropic J_c in a certain field and temperature range, see e.g. [39–41].

Yet, most of the attention has been focussed on YBCO thin films and much less is known about the other lanthanide-*RE*BCO compounds (*Ln*BCO). In particular, comparative studies from a single source are rare and focus often on the comparison of crystal structures [42] or T_c values [43] or both [44, 45] and less on the performance, i.e. critical current (densities), I_c (resp. J_c), at interesting points in the temperature-magnetic field matrix. Certainly, very detailed investigations of individual *Ln*BCO compounds have been reported, e.g. [46–48] and above all on GdBCO [49–51], but comparing such data with each other in order to define trends is problematic, especially when different deposition techniques are involved. The problem of comparability becomes most obvious when the growth of self-assembling nanostructures of the BMO_3 type (*M* transition metal) within the *RE*BCO matrix is examined. While PLD mostly leads to the formation of biaxially oriented nanoparticles and -rods, CSD tends to create randomly oriented particles of spherical shape. Those differences are caused by the different growth modes of the two techniques, which also lead to very distinct shapes of the grain boundaries (GB). The growth mode of PLD leads to columnar grains with straight GB perpendicular to the substrate interface; *ex-situ* deposition techniques, such as CSD, promote laminar grain growth resulting in rather meandering shapes [52].

Therefore, we optimised a number of different single-*RE*123 compounds and the according nanocomposites with $BaHfO_3$ (BHO) via a CSD approach: the well-established TFA-MOD (metal organic deposition of trifluoroacetates). Our objective was to determine trends for the phase formation windows and structural and physical properties and thus to evaluate their suitability for CSD-grown CCs. For production, low furnace temperatures are of interest for economic reasons and wide processing windows for improved reproducibility of the properties and therefore increased robustness of the process. For a comprehensive comparison, a wide range of *RE*BCO phases has been chosen from the largest *RE* element still known to form a stable superconducting *RE*123 phase, Nd, over Sm, Dy, Ho and Er, to the very small *RE* ion Yb. Those phases were compared to YBCO and GdBCO, for which we had obtained similar data in previous studies [35, 53]. Not part of the study were several *Ln* elements, whose corresponding *RE*123 phases are either metastable (La) or unstable (Ce, Tb),

not superconducting (Pr) or would be radioactive (Pm). Also not included were Eu and Tm, mostly for timely reasons, as well as Lu due to expected difficulties for single-phase growth. We chose BHO as nanoscale flux pinning centres due to our expertise and good experience with this secondary phase with respect to pinning enhancement and reduction of the macroscopic anisotropy [35, 49]. For the current study, the windows of the growth temperatures at a constant gas composition with an oxygen partial pressure pO_2 of 150 ppm have been accessed via inductively determined values of T_c and J_c. The record values of each system are compared to each other and brought into relation to structural characteristics, e.g. the *c*-axis parameter.

2. Experimental section

All *RE*BCO systems studied here, pristine and with additional BHO nanoparticles, required separate precursor solutions, which were prepared after the same recipe based on the well-established TFA-MOD approach [2, 53–55]: The acetates of *RE*, Ba, and Cu (>99.99%, *Alfa Aesar*) were dissolved in water in a 1:2:3 ratio, mixed with an excess of trifluoroacetic acid (TFAH, 99.5+%, *Alfa Aesar*) to enforce a high degree of conversion of the salts into the trifluoroacetates, and stirred until the last remains of metal-organic salt were dissolved. The solutions were concentrated by means of a rotary evaporator to yield a viscid residue, which was re-diluted in ultra-dry methanol (>99.9%, H_2O < 50 ppm, *Carl Roth*) and filled up to the final concentration of the rare earth of 0.25 mol l^{-1}. In the case of the nanocomposite solutions, additional hafnium(IV)-2,4-pentanedionate ($Hf(acac)_4$, 97+%, *Alfa Aesar*) and a similar molar amount of barium acetate were dissolved in water to enable a theoretical formation of 12 mol% BHO within the *RE*BCO films. After adjusting the concentration, very small amounts of acetylacetone relating to roughly 60 mol% with respect to the *RE* element (or 1.5 vol%) were added to the solutions in order to make them insensitive to impurities such as water [53]. The additive leads to a momentary precipitation of copper acetylacetonate, which dissolves readily and permanently after a few minutes in an ultrasonic bath. Hereafter, the solutions were filtered through PTFE with 0.2 μm pore size.

These solutions were spin-coated on cleaned 10 × 10 mm^2 (100)-oriented $LaAlO_3$ (LAO) or $SrTiO_3$ (STO) single crystal substrates with a rotation speed of 6000 rpm for 30 s, which leads to a final film thickness of (220 ± 20) nm. Subsequently, the films were heat-treated as described in [53], whereby the oxygen partial pressure pO_2 during the crystallization was kept at 150 ppm and the oxygen for the final oxygenation process was introduced after the oxygenation temperature of 450 °C had been reached. The cooling step between crystallization and oxygenation was carried out in dry nitrogen with the same pO_2 and gas flux as used during the film growth.

The superconducting characteristics of the films were analysed by inductive techniques: the self-field critical current density $J_{c,sf}$ at 77 K with a calibrated Cryoscan (*Theva*, 50 μV criterion), the transition temperature T_c by a self-designed and calibrated mutual inductance device. Here we show $T_{c,10}$, $T_{c,50}$ and $T_{c,90}$ which are defined as the temperatures at which the net induced voltage reaches 10, 50 and 90% of the value in the normal state. The layer thicknesses were determined by atomic force microscopy (AFM; Dimension Edge, *Bruker*) on 50 μm wide bridge structures. Those bridges were prepared by photolithography with an image reversal resist (AZ5214E, *Microchemicals*) and wet-chemical etching with an 0.6 wt% HNO_3 dilution. Structural features of the films were investigated by x-ray diffraction (XRD; D8 Discover, *Bruker*, Cu-K_α radiation) and scanning electron microscopy (SEM) with a low-resolution 'table-top' device (SH-5000P, *Hirox*, tungsten cathode, SE-detector, 10 kV acceleration voltage). The high-angle annular dark-field scanning transmission electron microscopy (HAADF STEM) images were taken at an *FEI* Titan probe C_s-corrected transmission electron microscope (TEM) operated at 200/300 kV [56, 57].

3. Results and discussion

Most of the newly investigated *RE*BCO phases with *RE* = Dy, Ho and Er show exactly the same behaviour on the two single-crystal substrates LAO and STO, which are commonly used for basic investigations, as did YBCO and GdBCO described in a previous study of ours [35]: The pristine phases show significantly better properties on LAO, while the nanocomposites with BHO prefer STO as substrate. This had been related to a loss of the chemical inertness of STO at higher temperatures (particularly above 760 °C), resulting in both T_c reduction through Ti permeation and growth of misoriented grains because of a deterioration of the structural integrity of the substrate interface. This problem occurs mainly in pristine films and can be avoided by LAO, which seems to be stable up to higher temperatures in the same growth conditions (pO_2). The nanocomposites, on the other hand, tend to form spherical BHO particles within the *RE*BCO matrix but also flat and wide-stretched structures at the interface covering a large percentage of the substrate. We assume that those particles limit the Ti diffusion into the *RE*BCO matrix and preserve the lattice information of the substrate due to a small lattice misfit to STO (<7%). On LAO, this misfit is significantly larger (>10%) leading to randomly oriented BHO particles at the interface with a disturbing impact on the film growth for nanocomposites on LAO. Therefore, we focus mostly on the data for pristine films grown on LAO and BHO nanocomposites on STO.

The images of DyBCO, HoBCO and ErBCO in figure 2 exemplify the typical macroscopic appearances of optimally grown films: All films are completely dense and homogeneous apart from a few surface decorations on pristine DyBCO and the nanocomposite of ErBCO. Especially smooth are the surfaces of the pristine phases with only a flat terrace architecture while the nanocomposites show some superficial trenches.

Cross-sectional HAADF STEM images of YBCO, DyBCO, HoBCO and ErBCO pristine films and BHO-nanocomposites confirm that all films are very dense throughout the entire layer, see figure 3. They also show quite similar microstructural landscapes in general. All films, except the HoBCO nanocomposite, contain RE_2O_3 nanoparticles in the volume. In YBCO and DyBCO, those particles either occur

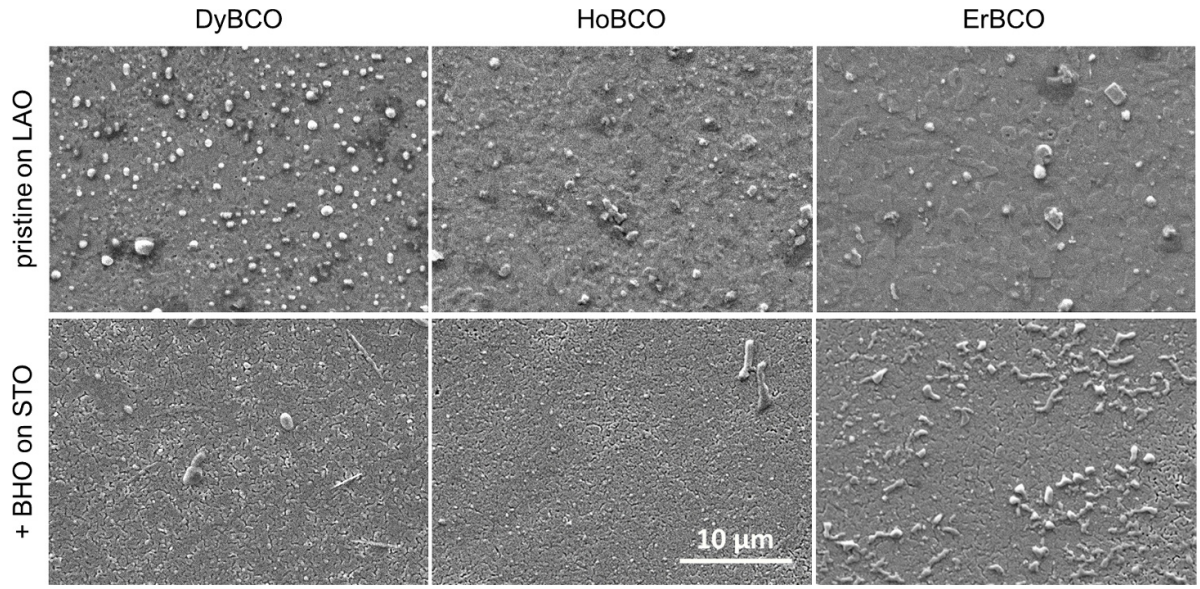

Figure 2. Structural film characteristics: plan-view images collected by a low-resolution SEM. Upper line shows pristine films, bottom line BHO-nanocomposites of DyBCO, HoBCO and ErBCO (from left to right).

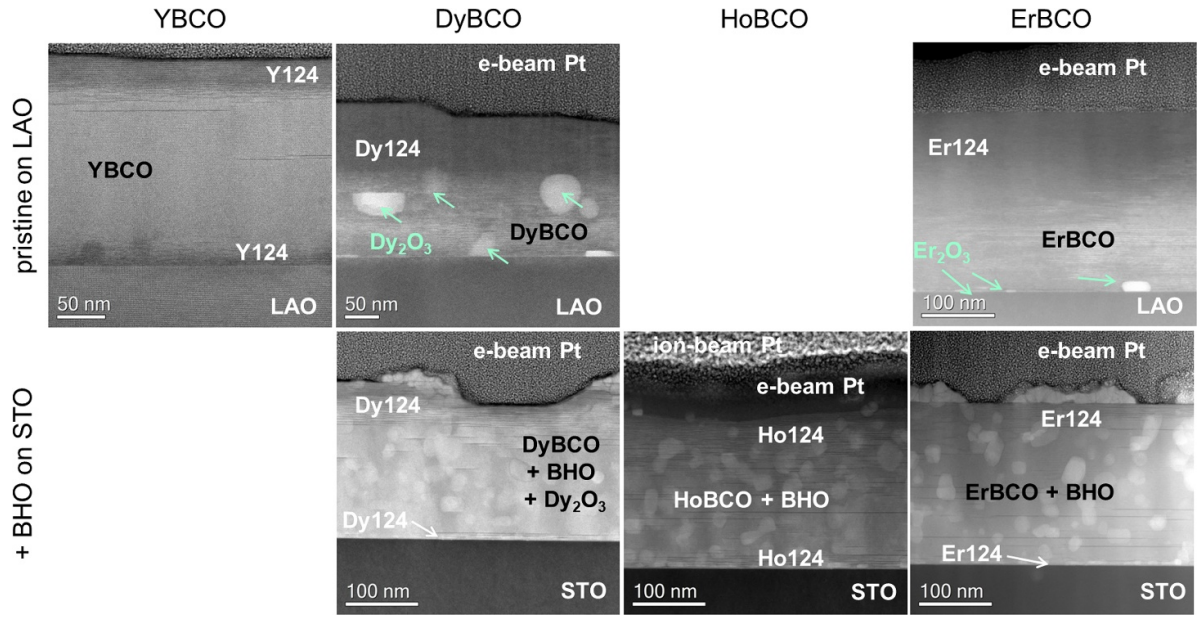

Figure 3. Microstructural features: HAADF STEM cross-sectional images. Upper line shows pristine films, bottom line BHO-nanocomposites of YBCO, DyBCO, HoBCO and ErBCO (from left to right).

in the middle part of the films or are attached to the substrate. Er_2O_3 on the other hand has only been found with association to the substrate. The presence of BHO does not play a role for RE_2O_3 particle size and distribution. Furthermore, BHO particle size and distribution are rather similar in all three studied cases. Aside from secondary phases, the bottom and top parts of the films contain a high density of elongated intergrowths that may be interpreted as additional Cu-O-planes or as insertions of $REBa_2Cu_4O_8$ (*RE*124). Those parts vary in thickness throughout the samples and are partly very thin, especially the bottom parts near the substrate. The middle parts are generally more sparsely interrupted by this type of stacking fault (SF). While such a graduation has been observed in all investigated systems, parts of the central films of pristine YBCO and DyBCO were even found nearly without SFs at all and in particular if no large secondary phase particles were present, as is shown on the example of pristine YBCO (top left picture in figure 3). ErBCO and DyBCO samples appear in some parts to have almost pure *RE*124 phases in the top part of the films, although this has not been detected by XRD (not shown) and is thus not really a pure phase but SFs of high density. In the BHO nanocomposites on STO, the amount of intergrowths seems to be lower, at least with respect to their dimension. The occurrence of stacking faults in direct vicinity

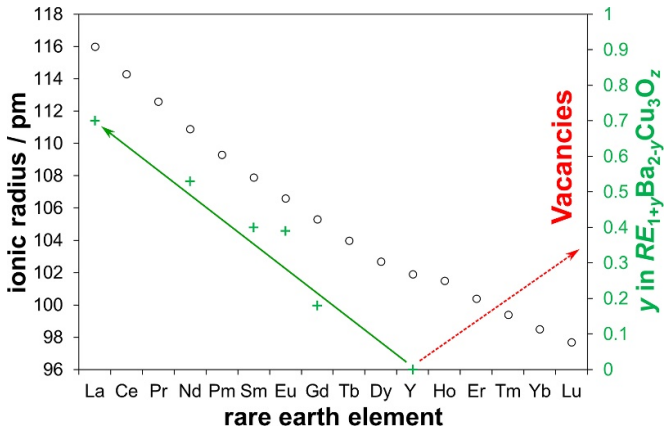

Figure 4. Rare earth ion size and phase stabilities: Shannon radii for RE^{3+} with 8-fold coordination [61], primary axis, black open circles, yttrium has been fit into the contracting line of lanthanides according to its size; increasing formation of a solid solution $RE_{1+y}Ba_{2-y}Cu_3O_z$ with increasing *RE* ion size beyond yttrium [59], secondary axis, green plus signs and solid line; scheme of the tendency to form vacancies with decreasing *RE* ion size beyond yttrium [58], red dotted line.

to the substrate interphase can be interpreted as a means of stress relief in the films, while the large number close to the film surfaces is believed to be a result of Cu accumulation during the film growth.

Despite several contradictions collected by MacManus-Driscoll *et al* in a thorough literature study [58], it is commonly agreed that the phase stabilities of the *RE*123 compounds differ significantly in dependence on the rare earth ion size, figure 4. While YBCO is known to form one of the most stable phases, mostly without any noticeable cation exchange in bulk materials [58], larger *RE* elements tend to form solid solutions through an exchange on the *RE* and Ba sites [59, 60] and smaller ions lead to vacancies in the lattice [58].

Both effects have significant implications for the *RE*BCO phase stabilities with obvious impact on the crystallisation temperatures, T_{cryst}, required for an optimal film growth via CSD as well as on the width of the T_{cryst} windows, figure 5: YBCO, the most stable phase, has the maxima for $J_{c,sf}$(77 K) at the lowest growth temperatures compared to the other *RE*BCO compounds, both for the pristine phases (~780 °C) and the nanocomposites (~770 °C). With falling and rising *RE* ion size, these optima shift towards higher growth temperatures, particularly in the case of pristine films on LAO, and the windows become incrementally narrower, particularly for the nanocomposites on STO. T_c values do not show as clear maxima as the J_c values, but YBCO and the adjacent compounds with similar *RE* ion sizes, HoBCO and DyBCO, span a rather large temperature window for very narrow transition widths ($\Delta T_c = T_{c90} - T_{c10}$). The smaller and larger *RE* ions, Er and Gd, show similarly narrow ΔT_c values only in a very small range of T_{cryst} ~ 10 °C, in some cases only at a distinct annealing temperature. This is most likely due to inhomogeneities in the films caused by disorder on the atomic scale (solid solution or vacancies), which reduces the reproducibility dramatically. Those very narrow windows, specifically of the GdBCO and ErBCO nanocomposites, may certainly be considered difficult with respect to CC fabrication. Nevertheless, previous results have also shown that other growth parameters, such as the pO_2, are further means to influence the quality and windows of the film growth. *RE*BCO phases with larger *RE* ions, e.g. GdBCO, profit from lower pO_2 [49].

The record T_c and J_c values achieved so far in every *RE*BCO system, regardless of BHO presence and including further samples grown with additional variations of the pO_2, are summarized in figure 6. Up to this point, the growth of NdBCO has not been successful yet despite a very thorough scan of the T_{cryst}–pO_2 matrix. None of the NdBCO samples shows any sign of superconductivity above 77 K. The x-ray diffraction patterns (not shown) give only very weak signs of the desired phase with poor *c*-axis texture but point towards very high optimal growth temperatures (>840 °C). This might be in conflict with the stability of the LAO substrate and the reason for the failing phase formation. Also SmBCO is more difficult than smaller *RE* ions. In contrast to NdBCO however, it forms the Sm123 phase without problems and with very dense and homogeneous films of good *c*-axis texture. Yet, the superconducting properties do not show the same reproducibility, which is attributed to the large stoichiometric disorder in the investigated films and, again, to an increasing influence of the substrate stability at the very high temperatures required for the film growth. Several SmBCO samples show very good properties, though, and the optimum temperatures seem to be ~830 °C for both pristine films and nanocomposites grown at pO_2 = 150 ppm. A reduction to 50 ppm slightly shifts the optima to 820 °C for both.

On the side of the smaller *RE* ions, YbBCO can be grown indeed, but it gives mostly broad transitions with a maximum $T_{c,90}$ of 89.5 K, figure 6(a). The optical appearance of the samples is already severely disturbed after the pyrolysis, which is in clear contrast to all the other *RE*BCO systems investigated here. From our experience with the sensitivity of YBCO and GdBCO towards humidity in the solutions and as-deposited gel-like films [53], we assume that YbBCO solutions are significantly more sensitive to traces of water, and the addition of acetylacetone may not have the same beneficial effect. Therefore, YbBCO seems to require a further optimisation of the solution preparation and pyrolysis, before the growth of high-quality films can be addressed.

Disregarding the problematic cases of the very small and large *RE* ions Yb and Nd, optimally grown *RE*BCO films from Sm to Er show a very narrow margin of T_c values ranging from 94.0 to 95.4 K, figure 6(a). Only YBCO drops out, which may be attributed to one or more of the following facts that distinguish Y from the other *RE* elements: Y is not a lanthanide, it is significantly lighter, and magnetic characteristics may play a role, too. Thus, a tendency of T_c solely related to the *RE* ion size as established in literature for bulk samples [62–64] is not observed in this investigation and may not even be expected since older studies suggest that also NdBCO [63] and YbBCO [65] can achieve T_c values of up to 96 K. A similar trend applies for the inductive values of $J_{c,sf}$ at 77 K, figure 6(b): The lanthanides seem to head for the same direction and maybe the same limits of about 6 MA cm^{-2}. The slightly lower values of

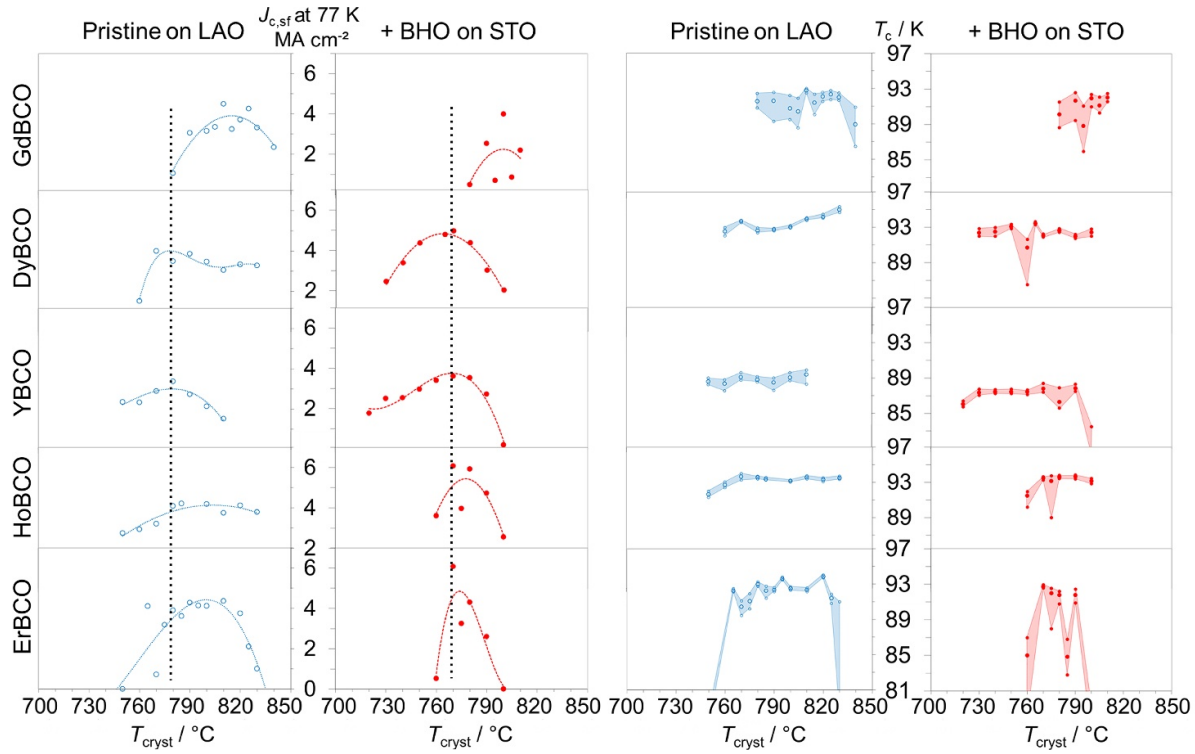

Figure 5. Windows of the crystallisation temperatures: inductively determined values of $J_{c,sf}$ at 77 K on the left side and T_c ($T_{c,90}$ as upper, $T_{c,10}$ as lower limits of the coloured area and $T_{c,50}$ as larger circles within the frame) on the right side, both over the crystallisation temperature for five *RE*BCO systems (*RE* = Gd, Dy, Y, Ho, Er with decreasing *RE* ion size top-down); the pristine phases on LAO are shown in blue, the nanocomposites on STO in red; the perpendicular lines in the J_c graphics mark the optima of YBCO, the most stable phase.

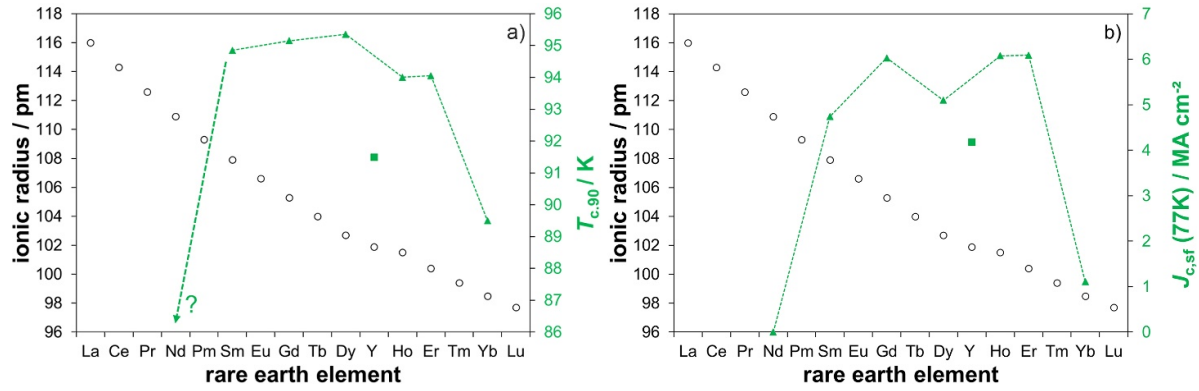

Figure 6. Record values: highest inductive values achieved so far (green, secondary axis) within the different *RE*BCO systems combining pristine films, nanocomposites and all variations of pO_2 during the crystallisation: (a) $T_{c,90}$; (b) $J_{c,sf}$ at 77 K; the primary axes show the trend of the *RE* sizes again to show that the middle-size element Y drops out of the line of lanthanides with respect to superconducting properties (square symbol).

DyBCO and SmBCO are rather a matter of statistics, but for the same reason the dropout of YBCO is real since more than a hundred samples have been prepared in this system over several years. However, 77 K is rather close to T_c, so the generally lower J_c values of YBCO can be considered a T_c effect.

Those record values shown in figure 6 may not be the absolute maxima possible but are presumably quite close to what can be achieved in thin films grown by CSD, particularly for T_c. One aspect that has been neglected for the present study though is the oxygenation process, namely conditions such as pO_2, annealing temperature and dwell time. This topic has been widely ignored for many years although those parameters are expected to have a significant impact on the oxygen load and with that on the lattice parameters as well as T_c and J_c. Yet, this topic seems to be very comprehensive on its own and is, therefore, under current investigation. All films shown here have been oxidised in the same way, i.e. the films were annealed in pure oxygen (p = 1 atm) at 450 °C for about 120 min. The rather high annealing temperature and long dwell time are expected to allow for fast and thus

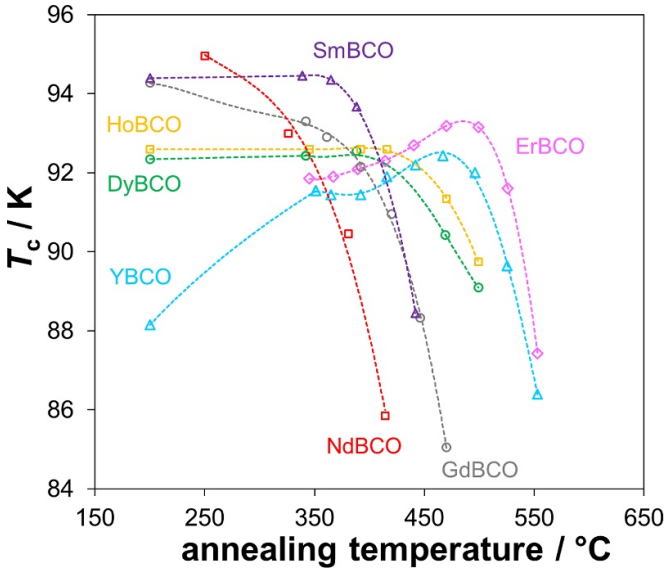

Figure 7. T_c vs. oxygenation temperature: dependence of T_c on the oxygen annealing temperature for different *RE*BCO phases with *RE* = Nd, Sm, Eu, Gd, Dy, Y, Ho, Er. Figure adapted from [66].

mostly complete oxygen diffusion processes in the films. Subsequently, all samples were furnace-cooled in this atmosphere, whereby the slow cooling rates let us assume that equilibria of the oxygenation may have been reached down to 300 °C–350 °C. According to literature, the *RE* species has indeed a severe influence on the oxygenation of the *RE*BCO phase, figure 7 [66, 67]. Yet, most of our systems seem to pass their respective optimum oxygenation temperature during the slow furnace-cool and may thus be considered optimally doped. Based on figure 7, only the two systems YBCO and ErBCO appear to have the potential for a further increase of T_c by quenching from the oxygen annealing temperature. Therefore, they may be slightly more in the overdoped region of the phase diagram due to the cooling in the furnace. However, aiming for their T_c maxima may even decrease rather than increase J_c since the J_c maximum had been found in the overdoped region [68–70].

In combination with T_c, the *c*-axis parameter is often used to estimate the oxygen doping level of YBCO, as e.g. shown in [71]. Yet, this is only strictly valid for single crystals and has rather little relevance for thin films, where many more factors influence both T_c and *c*, such as stoichiometry variations due to secondary phase precipitation, foreign-ion permeation from the substrate or artificial pinning centres, and above all strain induced by the substrate, misoriented grains or secondary phases [72]. Nevertheless, the thin films interestingly show very distinct relations between T_c and *c*, the latter determined via the Nelson–Riley method [73], figure 8. The green lines depict the theoretical values of *c* in single crystals for oxygen deficit $x = 0$, c^*, taken from the ICSD database. For YBCO, the entirety of data of superconducting films ever produced with CSD in our group forms a cloud around just this line of c^* and an average value of T_c, $ØT_{c,90}$, of roughly 87–88 K. Thus, a large number of samples is found with

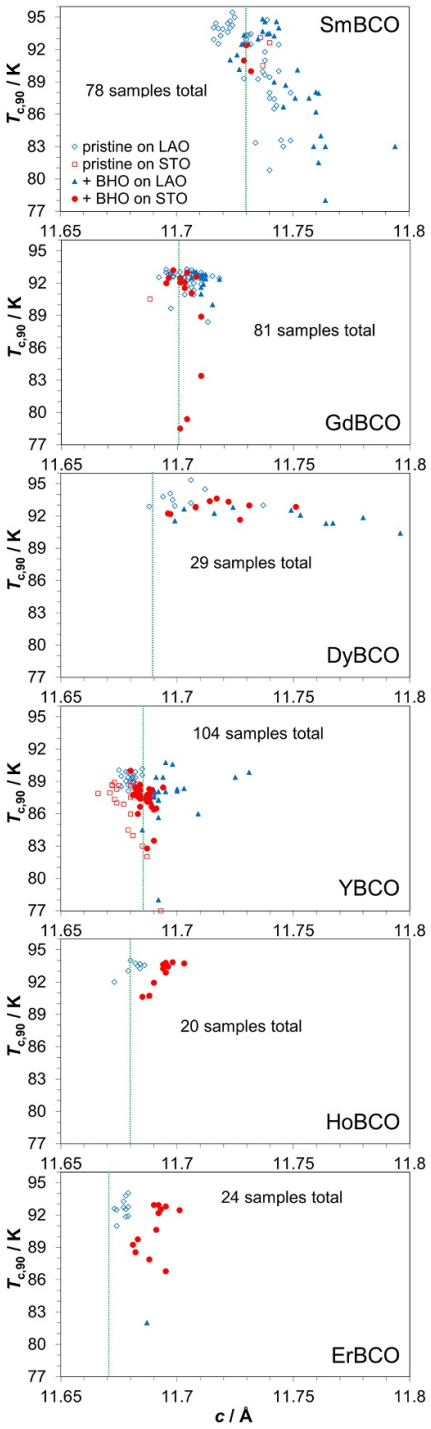

Figure 8. T_c vs. *c:* Dependence of $T_{c,90}$ on the lattice parameter *c* over all samples produced in the different *RE*BCO systems (*RE* = Sm, Gd, Dy, Y, Ho, Er), open symbols stand for pristine, solid for nanocomposites, blue on LAO, red on STO; the green lines mark the theoretical *c* value for $x = 0$ in single crystals.

$c < c^* = 11.686$ Å. Distinguishing between pristine films (open symbols) and nanocomposites (solid symbols) of YBCO, it is mostly the pristine samples with the very small values of $c < c^*$, whereby those films show a dramatic decrease of $T_{c,90}$ with *c* on STO (red open symbols) and form a very dense cloud

on LAO (blue open symbols) with $ØT_{c,90}$ ~ 89 K. The nanocomposites on STO (red solid symbols) also form a rather dense cloud around c^* with $ØT_{c,90}$ ~ 87.5 K; on LAO (blue solid symbols), c stretches out to significantly larger values, though, without a negative impact on $T_{c,90}$. The generally very small values of c, particularly in pristine samples, point to high oxygenation grades with x close to zero, which supports the idea that the films may be slightly overdoped as deduced from figure 7. However, further microstructural events beyond the oxygenation seem to occur in films with $c < c^*$ causing slight compressive strain in the c direction of the crystal structure.

The underlying databases for HoBCO and ErBCO with the smaller *RE* ions may contain considerably less samples, yet one difference is obvious: c is mostly larger than c^*. This suggests that the films are not as fully oxygenated as the YBCO films. Yet, strain caused by other reasons than oxygen vacancies may simply overcompensate and therefore mask the impact of oxygen loading on c. Comparable are the dense clouds with high T_c values for pristine films on LAO and the larger values of c for the nanocomposites.

In the direction of the larger *RE* ions, the T_c–c characteristics become more versatile. DyBCO shows nearly no T_c dependence on c, i.e. the c parameter extends from $c^* = 11.689$ Å towards very large values of 11.796 Å maintaining $T_{c,90}$ of at least 90.4 K. The widest span has the nanocomposite on LAO, even showing c-parameters as small as c^*; the pristine films on LAO have the narrowest range. It is very unlikely that the oxygenation grade is responsible for the expansion of c, since a strong impact on T_c should be expected. The reasons for the large c-axis parameters in DyBCO are not clear at present; yet, the high tolerance of T_c towards such an expansion of c is remarkable. GdBCO, on the other hand, shows a very dense data cloud again: almost all samples show c parameters very close to c^* and $ØT_{c,90} > 92$ K. Only a few T_c values drop out amongst the nanocomposites on STO. Yet another behaviour occurs in SmBCO, as this system shows a dramatic decrease of T_c for increasing c.

Some of the observations for the T_c–c correlation may have to remain uncommented, particularly the reasons for the severe differences between the large *RE* ions Dy, Gd and Sm, since too many factors may contribute. Yet, it can be concluded that the nanocomposites show wider ranges of the c parameter and generally larger values of c. Strain caused by the BHO nanoparticles is very unlikely the reason, since the strain fields around the particles are very narrow, as determined by TEM. Further, it cannot be concluded from our data that BHO generally suppresses T_c in CSD-grown films, as often observed in PLD-grown films [74–76]. In fact, for YBCO, the largest T_c values were found in nanocomposites. Thus, it is also unlikely that a diffusion of Hf into the *RE*BCO matrix causes the stretch of the c-axis in the nanocomposites, since it should come along with a simultaneous decrease of T_c [77]. Also, the lattice parameter c is rather expected to decrease, if Hf^{4+} substitutes for Y^{3+} in the crystal structure [77]. Up to what extent the strain caused by the lattice misfit to the substrate has part in the T_c–c correlation is also unclear at present, since all *RE*BCO systems lie on the same side of the misfit with respect to the two relevant substrates, figure 9: LAO induces compressive,

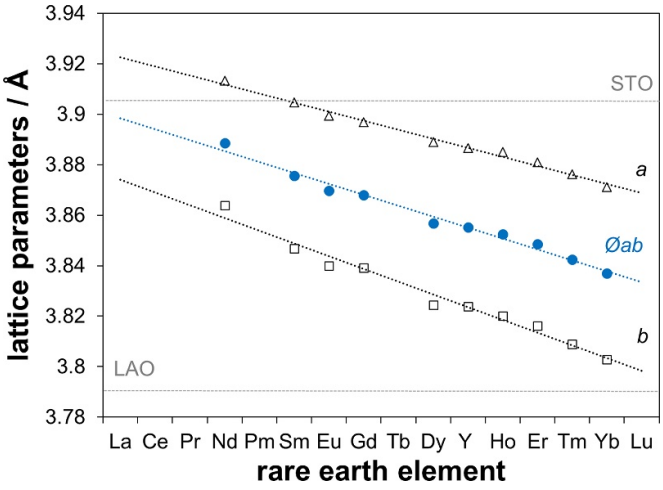

Figure 9. Lattice parameters: dependence of the *RE*BCO ($x = 0$) lattice parameters a (open triangles) and b (open squares) and their averages (solid blue circles) on the *RE* element, taken from the ICSD data base. The thin horizontal lines mark the lattice parameters of LAO and STO.

STO tensile strain in the *ab* direction of the *RE*BCO thin films, whereby the former increases with the *RE* ion size, while the latter decreases. Hence, similar impact on the c-parameters should be expected, i.e. an increasing expansion on LAO and a decreasing contraction on STO with increasing ion size. Such tendencies cannot be taken from the overall c-axis parameters of the investigated *RE*BCO-substrate combinations, also because only a very thin layer is directly concerned by the misfit to the substrate, and means of stress relief are applied in the films. More TEM analyses of different samples within one *RE*BCO system may have to be performed to clarify the reasons, specifically for the differences between the investigated systems.

4. Conclusions

Very similar microstructures were observed in CSD-grown films of different *RE*BCO compounds (*RE* = Sm, Gd, Dy, Y, Ho, Er), above all similar stacking fault distributions with a graduation through the layers, as well as similar secondary phases, sizes and distributions. The macroscopic film structure of all investigated systems is absolutely dense and homogeneous when optimally grown. Despite that, very interesting and partly unique relations between T_c and c were found. While most of the systems form rather dense data clouds around their respective theoretical c-axis values for $x = 0$, the lattice parameters of SmBCO and DyBCO scatter in a considerably wider range with a drastic decrease of T_c with increasing c in the case of SmBCO and only a marginal impact on T_c in the case of DyBCO. BHO nanocomposites show generally larger values and ranges of c, but mostly without a significant impact on T_c. The processing windows seem to follow a trend with lowest optima and widest ranges of the growth temperatures close to the optimal *RE* ion size, i.e. Y^{3+}. With increasing difference to it, the reproducibility for specific properties, such

as J_c and T_c, sinks noticeably due to enhanced disorder on the atomic scale. In particular, the growth windows of the nanocomposites with small or large *RE* ions are very narrow and must therefore be considered more difficult for CC production due to reduced process stability. Further, no tendencies were observed that could be related to solely the *RE* ion size or weight. Particularly, the non-lanthanide YBCO drops out of several characteristics. The *Ln*BCO compounds, on the other hand, head towards similar limits for $T_{c,90}$ ~ 95–96 K and $J_{c,sf}$ (77 K) ~ 6 MA cm^{-2} when fully optimised. The very small and large *RE* ions Yb and Nd require further optimisation beyond temperature and pO_2 adaption during the crystallisation step. Thereby, the substrate may play a crucial role for NdBCO, since temperatures beyond the stability of STO and LAO seem to be necessary, whereas YbBCO requires a re-formulation of the precursor solution or a modification of the pyrolysis, respectively, before the crystallisation step can be addressed adequately.

ORCID iDs

M Erbe https://orcid.org/0000-0001-9698-1509
P Cayado https://orcid.org/0000-0003-3703-6122
A Meledin https://orcid.org/0000-0002-3200-0553
J Hänisch https://orcid.org/0000-0003-2757-236X

References

[1] Wu M K, Ashburn J R, Torng C J, Hor P H, Meng R L, Gao L, Huang Z J, Wang Y Q and Chu C W 1987 Superconductivity at 93 K in a new mixed-phase Y–Ba–Cu–O compound system at ambient pressure *Phys. Rev. Lett.* **58** 908–10
[2] Gupta A, Jagannathan R, Cooper E I, Giess E A, Landman J I and Hussey B W 1988 Superconducting oxide films with high transition temperature prepared from metal trifluoroacetate precursors *Appl. Phys. Lett.* **52** 2077–9
[3] Matijasevic V, Rosenthal P, Shinohara K, Marshall A F, Hammond R H and Beasley M R 1991 Reactive coevaporation of YBaCuO superconducting films *J. Mater. Res.* **6** 682–98
[4] Singh R K and Kumar D 1998 Pulsed laser deposition and characterization of high-Tc $YBa_2Cu_3O_{7-x}$ superconducting thin films *Mater. Sci. Eng. R Rep.* **22** 113–85
[5] Christen H M 2001 Pulsed laser deposition of YBCO for coated conductor applications: current status and cost issues *Second-Generation HTS Conductors* (Berlin: Springer) pp 59–79
[6] Araki T and Hirabayashi I 2003 Review of a chemical approach to $YBa_2Cu_3O_{7-x}$-coated superconductors—metalorganic deposition using trifluoroacetates *Supercond. Sci. Technol.* **16** R71–94
[7] Xu Y L and Shi D 2003 A review of coated conductor development *Tsinghua Sci. Technol.* **8** 342–69
[8] Ma Y and Xiao L 2004 Second generation YBCO coated conductors: a review *Chin. Sci. Bull.* **49** 2435–9
[9] Knoth K, Engel S, Apetrii C, Falter M, Schlobach B, Hühne R, Oswald S, Schultz L and Holzapfel B 2006 Chemical solution deposition of $YBa_2Cu_3O_{7-x}$ coated conductors *Curr. Opin. Solid State Mater. Sci.* **10** 205–16
[10] Obradors X, Puig T, Ricart S, Coll M, Gazquez J, Palau A and Granados X 2012 Growth, nanostructure and vortex pinning in superconducting $YBa_2Cu_3O_7$ thin films based on trifluoroacetate solutions *Supercond. Sci. Technol.* **25** 123001
[11] Solovyov V, Dimitrov I K and Li Q 2013 Growth of thick $YBa_2Cu_3O_7$ layers via a barium fluoride process *Supercond. Sci. Technol.* **26** 013001
[12] Alfa Aesar (available at: https://www.alfa.com/de)
[13] Aktuelle Marktpreise für Seltene Erden - 2. Quartal 2018 (available at: https://institut-seltene-erden.de/aktuelle-marktpreise-fuer-seltene-erden-2-quartal-2018)
[14] Roas B, Schultz L and Endres G 1988 Epitaxial growth of $YBa_2Cu_3O_{7-x}$ thin films by a laser evaporation process *Appl. Phys. Lett.* **53** 1557–9
[15] Venkatesan T, Wu X D, Inam A and Wachtman J B 1988 Observation of two distinct components during pulsed laser deposition of high Tc superconducting films *Appl. Phys. Lett.* **52** 1193–5
[16] Wördenweber R 1999 Growth of high-Tc thin films *Supercond. Sci. Technol.* **12** R86–102
[17] Selvamanickam V, Xie Y, Reeves J and Chen Y 2004 MOCVD-based YBCO-coated conductors *MRS Bull.* **29** 579–82
[18] Palmer X *et al* 2015 Solution design for low-fluorine trifluoroacetate route to $YBa_2Cu_3O_7$ films *Supercond. Sci. Technol.* **29** 024002
[19] Obradors X *et al* 2006 Progress towards all-chemical superconducting $YBa_2Cu_3O_7$-coated conductors *Supercond. Sci. Technol.* **19** S13–26
[20] Skakle J M S 1998 Crystal chemical substitutions and doping of $YBa_2Cu_3O_x$ and related superconductors *Mater. Sci. Eng. R Rep.* **23** 1–40
[21] Ishida T 1987 Superconducting transition in the $Y_xEr_{1-x}Ba_2Cu_3O_{6+y}$ system *Jpn. J. Appl. Phys.* **26** L1540
[22] Cai C, Holzapfel B, Hänisch J, Fernández L and Schultz L 2004 High critical current density and its field dependence in mixed rare earth (Nd,Eu,Gd)$Ba_2Cu_3O_{7-\delta}$ thin films *Appl. Phys. Lett.* **84** 377–9
[23] MacManus-Driscoll J L *et al* 2004 Systematic enhancement of in-field critical current density with rare-earth ion size variance in superconducting rare-earth barium cuprate films *Appl. Phys. Lett.* **84** 5329–31
[24] Nurgaliev T, Miteva S, Nedkov I and Veneva A 1995 Magnetic characteristics of K-, Na- and Rb-doped YBCO ceramics *J. Magn. Magn. Mater.* **140–144** 1305–6
[25] Azoulay J, Lapsker I and Verdyan A 1996 Critical current density of Na doped YBCO thin films *Appl. Supercond.* **4** 35–39
[26] Lopes R F, Vieira V N, Mendoca A P A, Dias F T, da Silva D L, Pureur P, Schaf J and Jj R 2014 Low Sr doping effects on critical current density and pinning mechanism of YBa2Cu3O7-delta crystals *J. Phys.: Conf. Ser.* **568** 022014
[27] Tomé-Rosa C, Jakob G, Paulson M, Wagner P, Walkenhorst A, Schmitt M and Adrian H 1991 Thermally activated flux-flow in epitaxially grown $YBa_2(Cu_{1-X}Zn_X)_3O_7-$ thin films *Physica* C **185–189** 2175–6
[28] Horii S, Ichinose A, Ichino Y, Ozaki T, Yoshida Y, Matsumoto K, Mukaida M, Shimoyama J and Kishio K 2007 Critical current properties and microstructures in impurity-doped $ErBa_2Cu_3O_y$ films *Physica* C **463–465** 922–6
[29] Wang W T, Pu M H, Lei M, Zhang H, Wang Z, Zhang H, Cheng C H and Zhao Y 2013 Enhanced flux pinning properties in superconducting $YBa_2Cu_3O_{7-z}$ films by a novel chemical doping approach *Physica* C **493** 104–8
[30] Selinder T I, Helmersson U, Han Z, Sundgren J-E, Sjöström H and Wallenberg L R 1992 Yttrium oxide inclusions in $YBa_2Cu_3O_x$ thin films: enhanced flux pinning and relation to copper oxide surface particles *Physica* C **202** 69–74

[31] Luo Y Y, Wu Y C, Xiong X M, Li Q Y, Gawalek W and He Z H 2000 Effects of precursors with fine $BaZrO_3$ inclusions on the growth and microstructure of textured YBCO *J. Supercond.: Inc. Nov. Magn.* **13** 575–81

[32] MacManus-Driscoll J L, Foltyn S R, Jia Q X, Wang H, Serquis A, Civale L, Maiorov B, Hawley M E, Maley M P and Peterson D E 2004 Strongly enhanced current densities in superconducting coated conductors of $YBa_2Cu_3O_{7-x}$ + $BaZrO_3$ *Nat. Mater.* **3** 439–43

[33] Engel S, Thersleff T, Hühne R, Schultz L, Holzapfel B, Engel S, Thersleff T, Schultz L, Holzapfel B and Schultz L 2007 Enhanced flux pinning in $YBa_2Cu_3O_7$ layers by the formation of nanosized $BaHfO_3$ precipitates using the chemical deposition method *Appl. Phys. Lett.* **90** 102505–102505–3

[34] Matsushita T *et al* 2012 Improvement of flux pinning performance at high magnetic fields in $GdBa_2Cu_3O_y$ coated conductors with BHO nano-rods through enhancement of Bc2 *Supercond. Sci. Technol.* **25** 125003

[35] Erbe M *et al* 2015 $BaHfO_3$ artificial pinning centres in TFA-MOD-derived YBCO and GdBCO thin films *Supercond. Sci. Technol.* **28** 114002

[36] Varanasi C V, Barnes P N, Burke J, Brunke L, Maartense I, Haugan T J, Stinzianni E A, Dunn K A and Haldar P 2006 Flux pinning enhancement in $YBa_2Cu_3O_{7-x}$ films with $BaSnO_3$ nanoparticles *Supercond. Sci. Technol.* **19** L37–41

[37] Coll M *et al* 2014 Size-controlled spontaneously segregated Ba_2YTaO_6 nanoparticles in $YBa_2Cu_3O_7$ nanocomposites obtained by chemical solution deposition *Supercond. Sci. Technol.* **27** 044008

[38] Feldmann D M, Holesinger T G, Maiorov B, Foltyn S R, Coulter J Y and Apodaca I 2010 Improved flux pinning in $YBa_2Cu_3O_7$ with nanorods of the double perovskite Ba_2YNbO_6 *Supercond. Sci. Technol.* **23** 095004

[39] Palau A, Bartolomé E, Llordés A, Puig T and Obradors X 2011 Isotropic and anisotropic pinning in TFA-grown $YBa_2Cu_3O_{7-x}$ films with BaZrO3 nanoparticles *Supercond. Sci. Technol.* **24** 125010

[40] Petrisor T, Mos R B, Nasui M, Gabor M S, Augieri A, Celentano G, Felicis D D, Bemporad E, Ciontea L and Petrisor T 2014 The vortex path model analysis of the field angle dependence of the critical current density in nanocomposite $YBa_2Cu_3O_{7-x}$– $BaZrO_3$ films obtained by low fluorine chemical solution deposition *J. Supercond. Nov. Magn.* **27** 2493–500

[41] Miura M *et al* 2017 Tuning nanoparticle size for enhanced functionality in perovskite thin films deposited by metal organic deposition *NPG Asia Mater.* **9** e447

[42] Asano H, Takita K, Ishigaki T, Izumi F, Takayama-Muromachi E, Uchida Y and Watanabe N 1987 Neutron and x-ray diffraction studies of $RBa_2Cu_3O_{7-x}$ *Physica* B+C **148** 302–4

[43] Hor P H, Meng R L, Wang Y Q, Gao L, Huang Z J, Bechtold J, Forster K and Chu C W 1987 Superconductivity above 90 K in the square-planar compound system $ABaCuO_{6+x}$ with A=Y, La, Nd, Sm, Eu, Gd, Ho, Er and Lu *Phys. Rev. Lett.* **58** 1891–4

[44] Kaneko T, Toyoda H, Fujita H, Oda Y, Kohara T, Ueda K, Yamada Y, Nakada I and Asayama K 1987 Experiments on superconducting (rare earth)-$Ba_2Cu_3O_{7-\delta}$ down to 30 mK *Jpn. J. Appl. Phys.* **26** L1956

[45] Rao G V S *et al* 1987 High-Tc superconductivity in $Ln_{2-x}Ba_xCu_2O_5$ (1.0×1.6) and $LnBa_2Cu_3O_7$ (Ln=Dy, Er, Tm, Yb and Y) compounds *Physica* B+C **148** 237–8

[46] Ha H-S, Lee J-H, Ko R-K, Kim H-S, Kim H-K, Moon S-H, Park C, Youm D-J and Oh S-S 2010 Thick SmBCO/IBAD-MgO coated conductor for high current carrying power applications *IEEE Trans. Appl. Supercond.* **20** 1545–8

[47] Jia Q X, Foltyn S R, Coulter J Y, Smith J F and Maley M P 2002 Characterization of superconducting $SmBa_2Cu_3O_7$ films grown by pulsed laser deposition *J. Mater. Res.* **17** 2599–603

[48] Dürrschnabel M, Aabdin Z, Bauer M, Semerad R, Prusseit W and Eibl O 2012 $DyBa_2Cu_3O_{7-x}$ superconducting coated conductors with critical currents exceeding 1000 A cm^{-1} *Supercond. Sci. Technol.* **25** 105007

[49] Cayado P, Erbe M, Kauffmann-Weiss S, Bühler C, Jung A, Hänisch J and Holzapfel B 2017 Large critical current densities and pinning forces in CSD-grown superconducting $GdBa_2Cu_3O_{7-x}$–$BaHfO_3$ nanocomposite films *Supercond. Sci. Technol.* **30** 094007

[50] Horide T, Matsumoto K, Ichinose A, Mukaida M, Yoshida Y and Horii S 2007 Matching field effect of the vortices in $GdBa_2Cu_3O_{7-\delta}$ thin film with gold nanorods *Supercond. Sci. Technol.* **20** 303–6

[51] Iguchi T, Araki T, Yamada Y, Hirabayashi I and Ikuta H 2002 Fabrication of Gd–Ba–Cu–O films by the metal-organic deposition method using trifluoroacetates *Supercond. Sci. Technol.* **15** 1415–20

[52] Feldmann D M, Holesinger T G, Feenstra R and Larbalestier D C 2008 A review of the influence of grain boundary geometry on the electromagnetic properties of polycrystalline $YBa_2Cu_3O_{7-x}$ films *J. Am. Ceram. Soc.* **91** 1869–82

[53] Erbe M, Hänisch J, Freudenberg T, Kirchner A, Mönch I, Kaskel S, Schultz L and Holzapfel B 2014 Improved $REBa_2Cu_3O_{7-x}$ (RE = Y, Gd) structure and superconducting properties by addition of acetylacetone in TFA-MOD precursor solutions *J. Mater. Chem.* A **2** 4932–44

[54] McIntyre P C, Cima M J, Smith J A, Hallock R B, Siegal M P and Phillips J M 1992 Effect of growth conditions on the properties and morphology of chemically derived epitaxial thin films of $Ba_2YCu_3O_{7-x}$ on (001) $LaAlO_3$ *J. Phys. D: Appl. Phys.* **71** 1868–77

[55] Falter M, Häßler W, Schlobach B and Holzapfel B 2002 Chemical solution deposition of $YBa_2Cu_3O_{7-x}$ films by dip coating *Physica* C **372–376** 46–49

[56] Heggen M, Luysberg M and Tillmann K 2016 FEI Titan 80-300 STEM *J. Large-Scale Res. Facil. JLSRF* **2** 42

[57] Kovács A, Schierholz R and Tillmann K 2016 FEI Titan G2 80-200 CREWLEY *J. Large-Scale Res. Facil. JLSRF* **2** 43

[58] MacManus-Driscoll J L, Alonso J A, Wang P C, Geballe T H and Bravman J C 1994 Studies of structural disorder in $ReBa_2Cu_3O_{7-x}$ thin films (Re=rare earth) as a function of rare-earth ionic radius and film deposition conditions *Physica* C **232** 288–308

[59] Murakami M, Sakai N, Higuchi T and Yoo S I 1996 Melt-processed light rare earth element - Ba–Cu–O *Supercond. Sci. Technol.* **9** 1015–32

[60] Zhang K, Dabrowski B, Segre C U, Hinks D G, Schuller I K, Jorgensen J D and Slaski M 1987 Solubility and superconductivity in $RE(Ba_{2-x}RE_x)Cu_3O_{7+\delta}$ systems (RE=Nd, Sm, Eu, Gd, Dy) *J. Phys. C: Solid State Phys.* **20** L935

[61] Shannon R D 1976 Revised effective ionic radii and systematic studies of interatomic distances in halides and chalcogenides *Acta Cryst.* **A32** 751–67

[62] Xu Y, Guan W, Ata-Allah S S and Heiden C 1994 Rare earth ion size effect on Tc and ρn in the Ga and Zn doped $RBa_2Cu_{3-x}Ga_xO_{7-y}$ and $RBa_2Cu_{3-x}Zn_xO_{7-y}$ systems (R=Yb,Er,Y,Dy,Gd,Eu,Sm, and Nd) *Physica* C **235–240** 823–4

[63] Williams G V M and Tallon J L 1996 Ion size effects on 7 and interplanar coupling in $RBa_2Cu_3O_{7-\delta}$ *Physica* C **258** 41–46
[64] Lin J G, Huang C Y, Xue Y Y, Chu C W, Cao X W and Ho J C 1995 Origin of the R-ion effect on Tc in $RBa_2Cu_3O_7$ *Phys. Rev.* B **51** 12900–3
[65] Lee S C, Lee J H, Suh B J, Moon S H, Lim C J and Khim Z G 1988 Thermoelectric power and superconducting properties of $Y_1Ba_2Cu_3O_{7-\delta}$ and $R_1Ba_2Cu_3O_{7-\delta}$ *Phys. Rev.* B **37** 2285–8
[66] Shimoyama J, Horii S, Otzschi K and Kishio K 2001 How to optimize critical current performance of RE123 materials by controlling oxygen content *MRS Online Proc. Libr. Arch.* **689** E8.18
[67] Sato H 2018 Study on superconducting property in magnetic field of $Y_{1-x}Gd_xBa_2Cu_3O_{7-\delta}$ superconducting wire by nanostructure control *Dissertation* (Sekei: Sekei University)
[68] Feenstra R, Christen D K, Klabunde C E and Budai J D 1992 Role of oxygen vacancies in the flux-pinning mechanism, and hole-doping lattice disorder in high-current-density $YBa_2Cu_3O_{7-x}$ films *Phys. Rev.* B **45** 7555–8
[69] Strickland N M, Semwal A, Williams G V M, Verebelyi D T and Zhang W 2004 Optimizing the doping state of YBCO coated conductors *Supercond. Sci. Technol.* **17** S473–6
[70] Hänisch J, Storer J, Sheehan C, Coulter Y and Matias V 2007 Critical currents of overdoped Co-evaporated YBCO coated conductors *MRS Online Proc. Libr. Arch.* **1001** M14–04
[71] Liang R, Bonn D A and Hardy W N 2006 Evaluation of CuO_2 plane hole doping in $YBa_2Cu_3O_{6+x}$ single crystals *Phys. Rev.* B **73** 180505
[72] Hollmann E and Wördenweber R 2007 Analysis of defects in epitaxial oxide thin films via X-ray diffraction technology *Thin Solid Films* **515** 3530–8
[73] Menon E S K, Fox A G and Mahapatra R 1996 Accurate determination of the lattice parameters of γ-TiAl alloys *J. Mater. Sci. Lett.* **15** 1231–3
[74] Cantoni C, Gao Y, Wee S H, Specht E D, Gazquez J, Meng J, Pennycook S J and Goyal A 2011 Strain-driven oxygen deficiency in self-assembled, nanostructured, composite oxide films *ACS Nano* **5** 4783–9
[75] Tsuruta A, Yoshida Y, Ichino Y, Ichinose A, Matsumoto K and Awaji S 2014 $BaMO_3$ (M=Zr, Hf, Sn) material dependence of Tc reduction in $BaMO_3$-doped $SmBa_2Cu_3O_y$, films *J. Phys.: Conf. Ser.* **507** 022043
[76] Horide T, Kametani F, Yoshioka S, Kitamura T and Matsumoto K 2017 Structural evolution induced by interfacial lattice mismatch in self-organized $YBa_2Cu_3O_{7-\delta}$ nanocomposite film *ACS Nano* **11** 1780–8
[77] Elsabawy K M 2011 Superconductivity, structure visualization, mechanical strength promotion and Raman spectra of hafnium-doped-123-YBCO synthesized via urea precursor route *Cryogenics* **51** 452–9